

Multispectral Imaging Techniques for Monitoring Vegetative Growth and Health

Jonathan Gardner Weekley

Thesis submitted to the faculty of the Virginia Polytechnic Institute and State University in partial fulfillment of the requirements for the degree of

**Master of Science
In
Mechanical Engineering**

Alfred L. Wicks, Co-chair

Charles F. Reinholtz, Co-chair

Kathleen Meehan

Jerzy Nowak

December 4, 2007
Blacksburg, Virginia

Key Words: Computer Vision, Hyperspectral Imaging, Multispectral Imaging, Normalized Difference Vegetation Index, Vegetation Fluorescence

Multispectral Imaging Techniques for Monitoring Vegetative Growth and Health

Jonathan Gardner Weekley

Abstract

Electromagnetic radiation reflectance increases dramatically around 700 nm for vegetation. This increase in reflectance is known as the vegetation red edge. The NDVI (Normalized Difference Vegetation index) is an imaging technique for quantifying red edge contrast for the identification of vegetation. This imaging technique relies on reflectance values for radiation with wavelength equal to 680 nm and 830 nm. The imaging systems required to obtain this precise reflectance data are commonly space-based; limiting the use of this technique due to satellite availability and cost.

This thesis presents a robust and inexpensive new terrestrial-based method for identifying the vegetation red edge. This new technique does not rely on precise wavelengths or narrow wavelength bands and instead applies the NDVI to the visible and NIR (near infrared) spectrums in toto.

The measurement of vegetation fluorescence has also been explored, as it is indirectly related to the efficiency of photochemistry and heat dissipation and provides a relative method for determining vegetation health.

The imaging methods presented in this thesis represent a unique solution for the real time monitoring of vegetation growth and senesces and the determination of qualitative vegetation health. A single, inexpensive system capable of field and greenhouse deployment has been developed. This system allows for the early detection of variations in plant growth and status, which will aid production of high quality horticultural crops.

Acknowledgements

I would like to thank everyone who contributed to my graduate studies and this thesis.

Contents

CHAPTER 1 INTRODUCTION	1
1.1 MOTIVATIONS.....	1
1.2 THESIS OVERVIEW.....	2
CHAPTER 2 MULTISPECTRAL IMAGING	3
2.1 MULTISPECTRAL IMAGING	3
2.2 HYPERSPECTRAL IMAGING	3
CHAPTER 3 CHLOROPHYLL FLUORESCENCE	6
3.1 OVERVIEW.....	6
3.2 ELECTROMAGNETIC RADIATION.....	7
3.3 CHLOROPHYLL	8
3.4 FLUORESCENCE	10
3.5 PULSE MODULATED FLUORESCENCE MEASUREMENTS	11
3.6 FLUORESCENCE APPLICATIONS	12
3.6.1 <i>Fluorescence and Stress</i>	12
3.6.2 <i>Seeds and Food Quality Applications</i>	13
CHAPTER 4 MULTISPECTRAL RESULTS.....	15
4.1 MULTI-SPECTRUM FALSE COLOR	15
4.2 NDVI (NORMALIZED DIFFERENCE VEGETATION INDEX)	21
CHAPTER 5 VEGETATION FLUORESCENCE RESULTS.....	25
5.1 EQUIPMENT	25
5.1 VEGETATION FLUORESCENCE MEASUREMENTS	29
CHAPTER 6 CONCLUSIONS.....	36
6.1 NDVI (NORMALIZED DIFFERENCE VEGETATION INDEX)	36
6.2 VEGETATION FLUORESCENCE.....	37
REFERENCES.....	38

List of Figures

Figure 2.1. Reflectance profiles for lawn grass and brown silty loam.....	5
Figure 3.1 Energy values for visible spectrum electromagnetic radiation	8
Figure 3.2 Fluorescence quenching over a time period equal to one minute.....	10
Figure 4.1. Electromagnetic radiation reflectance profile for green vegetation	15
Figure 4.2. (left) Scene 1 (right) Scene 2	16
Figure 4.3. Scene 1 in the (a) NIR, (B) visible and (c) UVA spectrums.....	17
Figure 4.4. NIR spectrum image (left) grey-scale and (right) monochromatic red.....	18
Figure 4.5. Visible spectrum image (left) grey-scale and (right) monochromatic green.....	18
Figure 4.6 UVA spectrum image (left) grey-scale and (right) monochromatic blue.....	18
Figure 4.7 False color image created by combining monochromatic RGB images ..	19
Figure 4.8. False color results for (left) Scene 1 and (right) Scene 2.....	20
Figure 4.9. Color model threshold results for (left) Scene 1 and (right) Scene 2.....	20
Figure 4.10 NDVI values for vegetation, construction material and ice.....	22
Figure 4.11 Scene 1 visible spectrum image (left) and $NDVI^*$ solution (right).....	23
Figure 4.12 Scene 2 visible spectrum image (left) and $NDVI^*$ solution (right).....	23
Figure 5.1 Vegetation fluorescence measurement system.....	26
Figure 5.2 Original laser pointer package and laser diode electronics board.....	27
Figure 5.3 Laser diode control circuit.....	27
Figure 5.4. Non-IR radiation with a non-normal orientation passing through an interference filter	29
Figure 5.5. Visible spectrum image containing vegetation, white paper and an ebony imaging surface.....	30
Figure 5.6. Mean IR spectrum pixel values for dark current, vegetation, white paper and an ebony imaging surface.....	31
Figure 5.7. Sequential IR spectrum pixel values for dark current, vegetation, white paper and an ebony imaging surface.....	32
Figure 5.8. Threshold IR spectrum image containing vegetation, white paper and an ebony imaging surface.....	33

Figure 5.9. Vegetation under red light excitation in actinic light.....	33
Figure 5.10. Mean pixel values for vegetation during a red light excitation pulse (red) and under actinic excitation (green).	35

All figures created by Jonathan G. Weekley

Chapter 1 Introduction

1.1 Motivations

Electromagnetic radiation reflectance of vegetation, known as the red edge, increases significantly around 700 nm. The NDVI (Normalized Difference Vegetation index) is an imaging technique for quantifying red edge contrast for the identification of vegetation. This imaging technique relies on reflectance values for radiation wavelengths equal to 680 nm and 830 nm [7]. The imaging systems required to obtain this narrow reflectance data are commonly space-based; limiting the use of this technique due to satellite availability and cost [23].

The AVHRR (Advanced Very High Resolution Radiometer) is a multispectral imaging sensor suite associated with approximately one dozen NOAA (National Oceanographic and Atmospheric Administration) satellites. These sensor suites provide multispectral images for up to 6 electromagnetic radiation bands, including the visible and NIR (near infrared), at a cost of \$190 per scene [23].

This thesis presents a robust and inexpensive new terrestrial-based method for identifying the vegetation red edge. This new technique does not rely on narrow wavelength bands. Instead it applies the NDVI to the visible and NIR (near infrared) spectrums in toto.

The full spectrum NDVI methods developed here can be used in conjunction with a single, inexpensive imaging system to indirectly calculate LAI (leaf area index) values for field and green house canopies. These measurements can aid in the proper adjustment of irrigation algorithms, pest control methods, nutrient applications and other critical crop maintenance parameters [12].

The ability of the full spectrum NDVI imaging system to measure vegetation fluorescence has also been explored. Vegetation fluorescence is indirectly related to the efficiency of photochemistry and heat dissipation and provides a relative method for determining vegetation status.

1.2 Thesis Overview

Multispectral and hyperspectral imaging techniques and applications are discussed in Chapter 2. The required equipment and analysis methods for extracting meaningful data from multispectral and hyperspectral imaging systems is also covered. Chapter 3 provides an overview of electromagnetic radiation and its molecular interaction with chlorophyll. A unique multispectral imaging system and adjusted NDVI are proposed in Chapter 4. Results for differentiating between vegetation and non-vegetation within a digital image using an adjusted NDVI are compared with other thresholding techniques. Chapter 5 discusses the feasibility of using the proposed multispectral imaging system presented in Chapter 4 for the measurement of vegetation fluorescence and, therefore, qualitative monitoring of vegetation health. Lastly, conclusions and recommendations for future improvements to the new multispectral imaging system are discussed in Chapter 6.

Chapter 2 Multispectral Imaging

2.1 Multispectral Imaging

Multispectral imaging is a remote earth sensing technique for identifying surface objects and anomalies. The UVA (ultra-violet α) (320 nm – 400 nm), visible (400 nm – 700 nm), near-infrared (NIR) (700 nm – 1100nm), short wave infrared (1.1 μm – 2.5 μm), medium wave infrared (3 μm – 5 μm) and thermal infrared (8 μm – 14 μm) spectrums are typically employed in multispectral imaging systems [7]. Individual sensors are not necessary for the sensing of each spectrum; however, the utilization of multiple imaging sensors is required. These imaging sensors produce grey-scale images which can then be falsely colored and combined to extract meaningful information; an RGB (red-green-blue) scheme is typically employed.

Multispectral imaging has been used to study soil texture [2], detect landmines [24] and monitor vineyard quality [12]. A highly successful multispectral imaging system is maintained by NASA. The Landsat 7 satellite carries multispectral imaging sensors which continue to aid in the remote monitoring of agriculture, de-forestation, mineral resources and water resources.

2.2 Hyperspectral Imaging

Hyperspectral imaging is a higher resolution form of multispectral imaging. Hyperspectral imaging records absorption data for many narrowly defined spectral bandwidths, resulting in a continuous spectral absorption profile. An imaging system sensing 100 or more bands is generally referred to as hyperspectral.

Off-the-shelf hyperspectral imaging equipment for the UVA, visible and NIR is quite expensive; typically between \$2000 and \$20000 [18]. These systems use a focusing lens, prism-grating-prism and collimating lens. Prisms and gratings disperse and diffract incident light; separating it into narrow electromagnetic bands that are subsequently detected by a CCD. Hyperspectral imaging data are most commonly represented as reflectance, transmission or absorption graphs.

The USGS (United States Geological Survey), JPL (Jet Propulsion Laboratory) and JHU (John Hopkins University) maintain free reflectance libraries. Collectively, these libraries contain reflectance data for ice, man-made objects, minerals, rocks, vegetation and water.

Molecular species produce unique spectral reflectance profiles. These unique profiles are a result of molecule specific nuclei-electron-photon interactions [16] and can be used for object classification [7]. The reflectance profile for green lawn grass and brown silty loam is presented in Figure 2.1. These reflectance profiles highlight the unique absorption characteristics of terrestrial compounds.

The dramatic increase in green lawn grass reflectance between 700 nm and 800 nm is known as the vegetation red edge. The NDVI (Normalized Difference Vegetation Index) utilizes this red edge to differentiate between vegetation and non-vegetation.

Hyperspectral spectroscopy is used in military, industrial and agricultural applications. Face recognition [20], plant identification [17], fruit firmness and sugar content determination [13] [14], soil variability [9], soil texture [2] and the impact of nitrogen and environmental conditions on corn have been studied using hyperspectral imaging techniques [21].

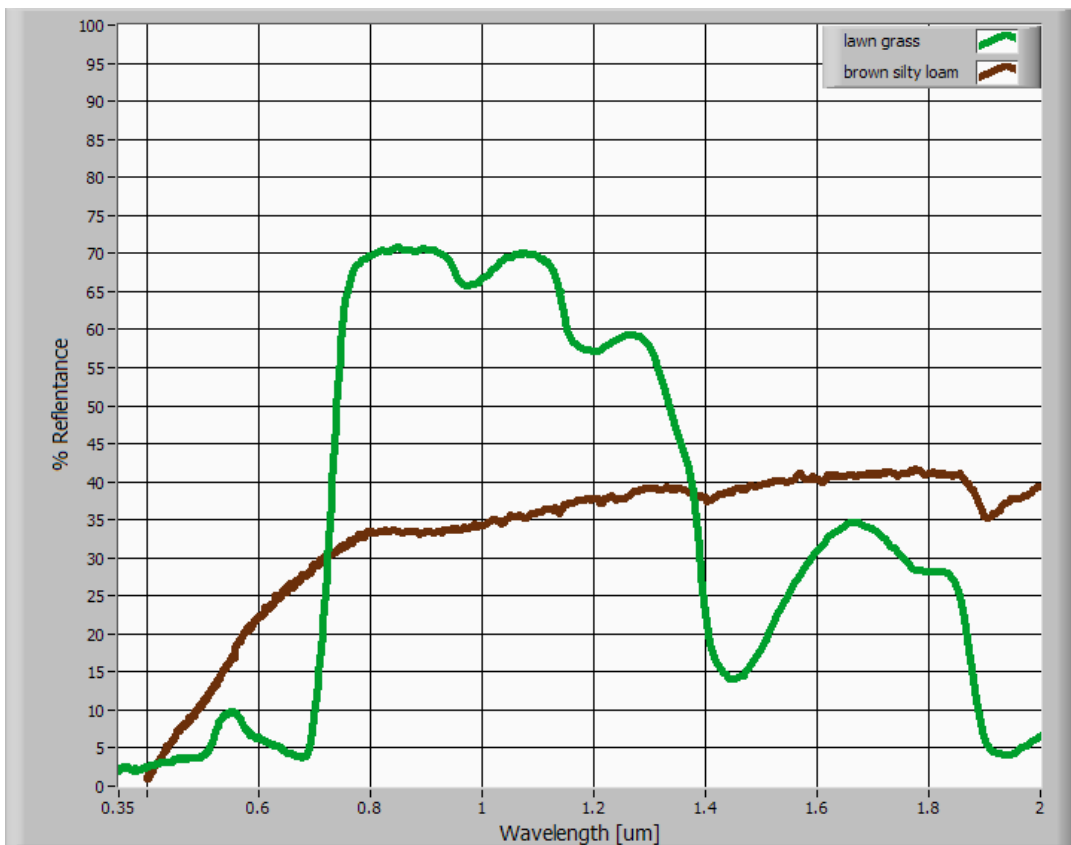


Figure 2.1. Reflectance profiles for lawn grass and brown silty loam.

Chapter 3 Chlorophyll Fluorescence

3.1 Overview

In association with carotenoids, chlorophyll harvests light energy to drive photosynthesis in two photosynthetic systems. Under actinic illumination chlorophyll fluoresces in the red and infrared which explains why vegetation appears bright in infrared photography.

When dark-adapted chlorophyll is illuminated, a significant increase in fluorescence occurs. The underlying processes and efficiency of photosynthetic systems can be studied by comparing dark-adapted chlorophyll fluorescence with fluorescence under actinic illumination. Chlorophyll fluorescence techniques allow determination of the relative photochemical response to stress conditions, seed sorting [10] [11] and post-harvest quality of fruit and vegetables [4].

Companies such as Turner Designs offer existing fluorometer solutions [22]. These designs utilize blue and green LEDs (light emitting diodes) and are available in bench-top and hand-held forms. As an example, Turner Designs' 10-AU Field Fluorometer is capable of long-term data logging and is packaged in a, rather large, water tight casing ($9.5\text{in} \times 21.7\text{in} \times 13.4\text{in}$). Moreover, the equipment has been designed for monitoring phycocyanin, phycoerythrin, oil and other biologically significant compounds in an aquatic setting; not for monitoring the stress of high-value horticultural crops. Inexpensive, field-deployable fluorometers for measuring crop fluorescence are not readily available.

In this chapter the fundamental principles of electromagnetic radiation are overviewed. The chlorophyll molecule is dissected, measurement of its fluorescence methods and techniques are presented and their applications are reviewed.

3.2 Electromagnetic Radiation

Electromagnetic radiation (ER) drives photosynthesis. The ER consists of an oscillating electric field and magnetic field and exhibits both particle and wave properties. The interaction of the electric and magnetic fields sustain and propagate ER.

The velocity at which an electromagnetic wave propagates through space is directly related to its frequency and wavelength and is equal to the speed of light ($3.0 \times 10^8 \text{ m/s}$) in a vacuum. Therefore, short wavelength radiation oscillates at higher frequencies than long wavelength radiation.

$$v = \lambda f \quad (3.1)$$

Furthermore, electromagnetic radiation is a non-continuous stream of energy packets; termed photons. Photons contain a specific quantity of energy and are also referred to as quantums. The energy of an electromagnetic wave is equal to Plank's constant multiplied by the frequency of the light wave.

$$E = hf = \frac{hv}{\lambda} \quad (3.2)$$

Where h is Plank's constant ($6.626 \times 10^{-34} \text{ J} \cdot \text{s}$), v is the velocity of the electromagnetic wave and λ is its wavelength. Accordingly, short length electromagnetic waves will possess more energy than long length electromagnetic waves.

PAR (photosynthetically active radiation) begins at approximately 700 nm and spans through 400 nm. These wavelengths represent energy between $1.75eV$ and $3.10eV$ respectively (Figure 3.1).

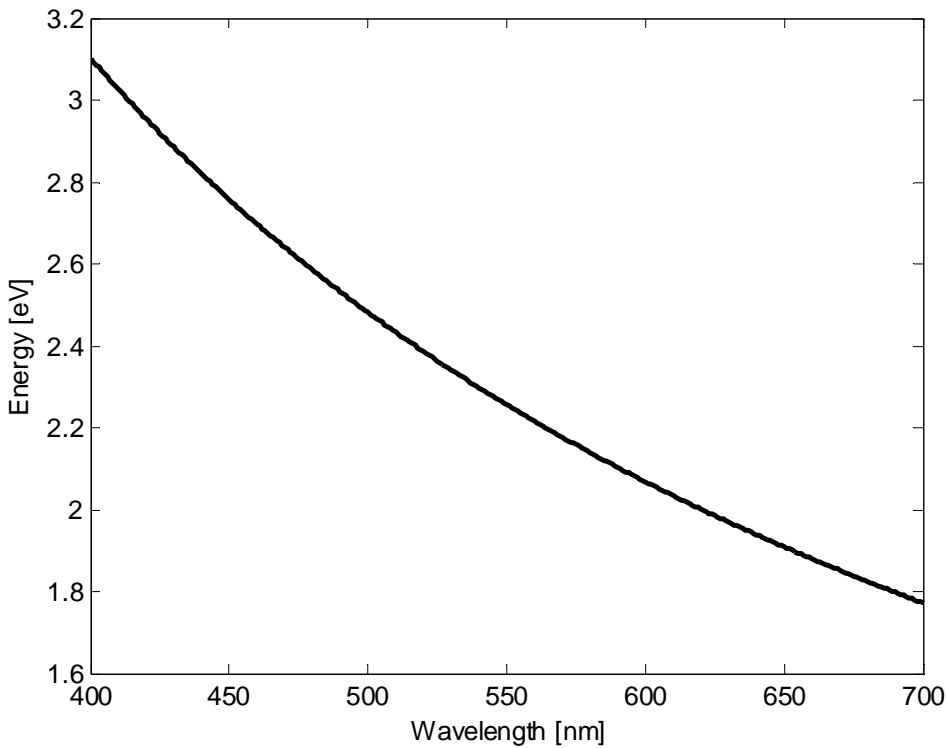


Figure 3.1 Energy values for visible spectrum electromagnetic radiation

3.3 Chlorophyll

Chlorophyll molecules are chlorine containing pigments found in all photosynthetic organisms [16]. These chlorophyll molecules are organized around protein complexes, known as photosystems, which harvest light energy to drive photosynthesis. Photosystems II and I are associated with the absorption of electromagnetic radiation with wavelength 680 nm and 700 nm respectively.

Though approximately fifty unique chlorophylls have been identified, chlorophylls *a* and *b* are the most important for photosynthesis [4]. The ratio of chlorophyll *a* to *b* is approximately 3 to 1. Chlorophyll *b* passes all of its energy to chlorophyll *a* and does not fluoresce. Thus, chlorophyll *a* is a molecule of interest with respect to chlorophyll fluorescence analysis.

Chlorophyll molecules are excited through the absorption of a discrete quantity of energy. When excited, a molecule moves from ground state to a higher energy state.

Chlorophyll fluorescence occurs when de-excitation from a higher energy state to ground state releases a photon. Because of heat and vibrational losses, fluoresced light has a longer wavelength than that of the exciting light. Specifically, chlorophyll *a* absorbs PAR and fluoresces in the red and near infrared.

Since photons represent discrete quantities of energy, electromagnetic radiation is a convenient and non-invasive method for exciting chlorophyll molecules.

Chlorophyll *a* has peak absorption bands in the blue and red regions of the electromagnetic spectrum. However, molecules at higher energy states relax to the first excitation level above ground within several pico seconds, which is too rapid to facilitate fluorescence. Therefore, a chlorophyll molecule under blue light excitation quickly falls to the intermediate energy state, which has a longer lifetime. When the chlorophyll molecule relaxes from this state back to the ground state, the energy difference between these states is emitted as red light.

The red absorption band for chlorophyll *a* begins at 680 nm and spans up through 650 nm. These wavelengths possess energy capable of exciting chlorophyll. However, the maximum red absorption for chlorophyll *a* occurs at 662 nm; therefore, light sources centered about 662 nm are appropriate for measurements of chlorophyll fluorescence [16]. The quantity of energy possessed by a wavelength of 662 nm is approximately 1.87eV .

Chlorophyll *a* fluoresces at wavelengths between 650 nm and 750 nm when excited with red light, with a maximum fluorescence peak centered about 666nm. A lesser peak centered about 728 nm also occurs [16].

The red absorption band for chlorophyll *b* begins at 660 nm and spans up through 600 nm, with maximum red absorption occurring at approximately 625nm. Therefore, chlorophyll *b* will absorb radiation intended for chlorophyll *a* when red light excitation is utilized.

3.4 Fluorescence

Light energy harvested by chlorophyll is used for (1) photochemistry, (2) dissipated as heat or (3) re-emitted as fluorescence. These three energy routes are mutually exclusive; therefore, an electron used to drive photosynthesis cannot be released as heat or re-emitted as fluorescence. Because of this, the amount of fluorescence is indirectly related to photochemistry and heat dissipation.

A significant increase in chlorophyll fluorescence occurs when dark-adapted chlorophyll is exposed to light. However, this increase in fluorescence rapidly decreases after approximately one second and reaches steady state after several minutes (Figure 3.2) [15]. This return to steady-state is a result of photochemical quenching and non-photochemical quenching and is termed fluorescence quenching.

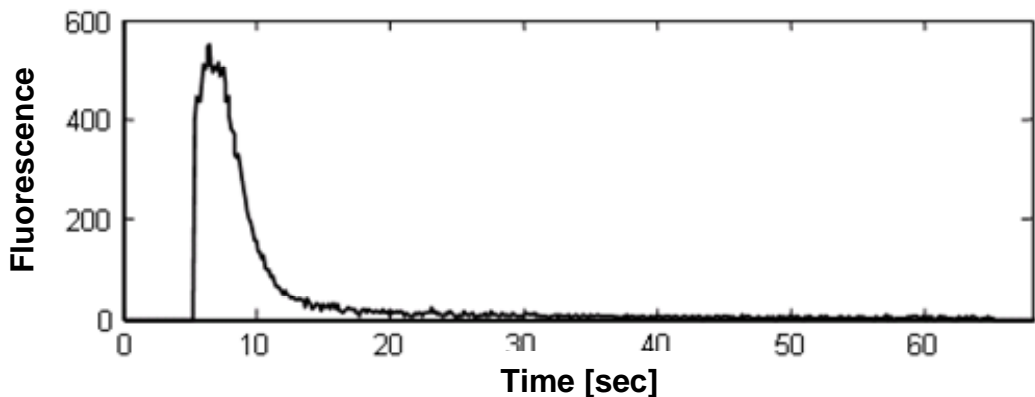


Figure 3.2 Fluorescence quenching over a time period equal to one minute.

Photochemical quenching, also known as photo-bleaching, is a result of an increase in electron transport in the photosynthetic reaction centres. When dark-adapted chlorophyll is illuminated, primary plastquinone electron acceptors become saturated and are not able to accept additional electrons. As the primary electron acceptors pass electrons to secondary acceptors, they are able to accept additional electrons and a decrease in fluorescence occurs.

Non-photochemical quenching is linearly related to heat dissipation efficiency relative to a dark-adapted state. Non-photochemical quenching is a product of fast

relaxing high energy state quenching and state transition, and slow relaxing photo-inhibition. These processes are affected by light induced damage and photo-protective processes [15].

3.5 Pulse Modulated Fluorescence Measurements

Modulated chlorophyll fluorescence measurements begin by obtaining a measurement for minimal fluorescence, F_0 . In laboratory settings this measurement is taken under minimal illumination with a measuring light. In the field, minimal fluorescence can be measured during pre-dawn hours.

The dark-adapted chlorophyll is then exposed to a pulse of excitation light and the maximum fluorescence is measured, F_m . In a dark-adapted state a maximum number of the primary chlorophyll electron acceptors are un-occupied. When the excitation light is pulsed, these electron acceptors become occupied concurrently and subsequent electrons are available for fluorescence. Therefore, maximum fluorescence is measured when a maximum number of electron acceptors within the photosynthetic reaction centres are saturated.

The chlorophyll is then illuminated with actinic light. In a field situation this requires waiting for daylight. In the laboratory a lamp with an appropriate emission spectrum is sufficient. The excitation light is then pulsed to measure maximum fluorescence under actinic illumination, F'_m . Steady-state fluorescence, F_t , is the level of fluorescence, under actinic illumination, just prior to an excitation pulse. Measurements of steady state and maximum fluorescence under actinic light can be compared with maximum dark-adapted fluorescence measurements to determine photosynthetic efficiencies.

Minimum and maximum fluorescence is greatly affected by soil conditions, stress levels and light acclimation. Furthermore, the absorption band for chlorophyll *a* partially overlaps the fluorescence emission spectrum. Therefore, a percentage of fluoresced light will be re-absorbed by the chlorophyll. Stress level and re-absorption characteristics vary

widely intra-plant and plant-to-plant and, therefore, comparison of these fluorescence measurements will not result in meaningful data.

Additionally, *in vivo* fluorescence measurements represent the interactive characteristics of all molecules present in the vegetation tissue. Vegetation contains chlorophylls, as well as proteins, lipids, water and other biologically significant molecules. The effect of these additional molecules is to shift the red absorption and fluorescence bands for chlorophyll *a* to longer, less energetic wavelengths [16]. Experimental results presented in Chapter 5 represent fluorescence signatures for vegetation in toto, and not chlorophyll *a* fluorescence exclusively.

3.6 Fluorescence Applications

3.6.1 Fluorescence and Stress

Chlorophyll fluorescence represents a real-time, non-destructive method for determining the relative efficiency of Photosystem II, *in vivo*, under stress conditions. Photosystem II harvests light energy at 680 nm, and the efficiency with which this light energy is absorbed is directly related to the overall efficiency of photochemistry. Photochemical quenching can be measured in terms of the quantum yield of PSII $\Phi_{PSII} = (F'_{m'} - F_t) / F'_{m'}$, the proportion of open PSII reaction centres $qP = (F'_{m'} - F_t) / (F'_{m'} - F'_{0'})$ and the maximum quantum yield of PSII $F_v / F_m = (F_m - F_0) / F_0$ through the comparison of fluorescence measurements. Non-photochemical quenching, $NPQ = (F_m - F'_{m'}) / F'_{m'}$, due to fast relaxing high energy state quenching and state transition and slow relaxing photo-inhibition can also be studied through fluorescence measurements. Non-photochemical relaxation processes reflect the efficiency at which energy is converted to heat and provide information concerning photo-protective processes.

Photochemical quenching is related to maximum dark-adapted fluorescence, steady-state fluorescence under actinic illumination and minimum fluorescence under

dark-adaptation and actinic illumination. Non-photochemical quenching is related to maximum dark-adapted fluorescence and maximum fluorescence under actinic illumination.

The response of PSII to atmospheric pollutants, climate change, drought, fire damage, freezing, heavy metals, herbicides, light intensity, nitrogen oxide, sulfur dioxide and temperature extremes have been studied using chlorophyll fluorescence [4]. Chlorophyll fluorescence has been used to study these effects on photosynthetic efficiency relative to normal photosynthetic efficiencies; not to identify specific stress *in vivo*.

3.6.2 Seeds and Food Quality Applications

High value horticulture production requires access to high quality seeds. Seed size, weight, color and moisture content are characteristics commonly used to determine viability [8]. Seed size does not vary greatly intra-species; less than half an order of magnitude [6]. Heavier seeds are preferred because they are well developed [8]. Green, immature seeds contain chlorophyll and are less likely to germinate. Seed moisture content largely influences storage robustness. For these reasons, sorting provides a method for delivering high quality seeds to the agricultural community.

The Commonwealth of Virginia regulates the labeling and advertising of seeds through the Virginia Seed Law. The VOPI (Virginia Office of Product and Industry Standards) enforce the Virginia Seed law by randomly testing seeds to ensure the accuracy of manufacturer labels. In an effort to further improve seed quality the VCIA (Virginia Crop Improvement Association) maintain minimum germination rates for several high value agricultural crops. Specifically, VCIA will certify seeds meeting the following criteria: peanuts (85%), barley and oats (90%), wheat and rye (85%) and soybean (80%).

Common methods for determining seed quality are time consuming and destructive. Hyperspectral imaging and chlorophyll fluorescence are quick, non-destructive techniques for seed sorting.

Chlorophyll fluorescence signatures are directly related to seed maturity. Seed sorted using chlorophyll fluorescence has germination rates up to 100% (compared with a 95% germination rate for non-sorted seeds) [10] [11]. This increase in viability was also observed after controlled deterioration [11].

Fluorescence techniques have also been used to non-destructively quantify the quality of packaged produce. For instance, the quality of broccoli packaged in modified atmosphere packaging can be ascertained [4].

Chapter 4 Multispectral Results

4.1 Multi-Spectrum False Color

The electromagnetic reflectance profile for green vegetation includes a dramatic increase between the wavelengths of 700 nm and 800 nm. Consequently, vegetation appears relatively dim in the UVA and visible spectrums and bright in the NIR spectrum. By comparing UVA and visible spectrum images with NIR spectrum images vegetation should become distinguishable from non-vegetation. Therefore, a unique multispectral imaging system which utilizes the UVA, visible and NIR spectrums in toto is proposed for differentiating between vegetation and non-vegetation within a scene. The proposed imaging system includes a monochromatic digital camera sensitive to the UVA, visible and NIR spectrums in combination with three manually interchangeable band pass filters.

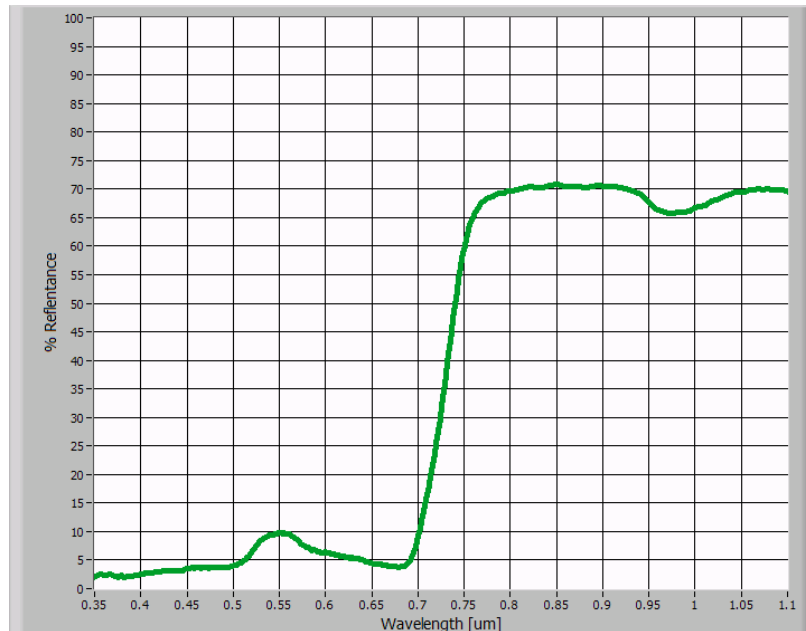


Figure 4.1. Electromagnetic radiation reflectance profile for green vegetation

Experiments were conducted to verify the performance of the proposed multispectral imaging system for differentiating between vegetation and non-vegetation within a scene. System components and experimental results are subsequently presented.

A B+W #093 infrared-pass glass filter capable of passing radiation with wavelengths greater than 700 nm was used to capture NIR images. A B+W #403 UVA-pass glass filter capable of passing wavelengths between 325 nm and 385 nm was used to capture UVA images. The UVA-pass filter is designed to block visible spectrum radiation and most NIR radiation. The filter contains a transmittance “hump” centered at 725 nm. Therefore, UVA images captured with the UVA-pass filter will contain a small amount of NIR reflectance information. Visible images were captured with a B+W #486 UV/IR blocking glass filter [1].

The Sony XCD-X710 IEEE-1394 Firewire camera was used as the monochromatic imaging sensor. The camera was purchased through Edmund Optics. This camera uses a one-third inch progressive scan IT CCD with a 600×800 pixel resolution and a pixel depth of 10 bits. The Sony XCD-X710 is sensitive to electromagnetic radiation with wavelengths between approximately 300 nm and 1000 nm; with peak sensitivity occurring at approximately 500 nm [5].

National Instruments LabView software was used to interface with the Sony XCD-X710 and to process image frames. LabView was chosen for its robust vision capture and image processing capabilities. Programs were authored to record, process, store and display image frame data.

Spectral images were captured with the camera mounted atop a stationary platform. This fixed camera position ensured that spectrum images uniformly represented a given scene. Two unique scenes were chosen for the experiment; with each scene containing approximately equal amounts of vegetation and non-vegetation.



Figure 4.2. (left) Scene 1 (right) Scene 2

NIR, visible and UVA spectrum images for Scene 1 are presented in Figure 4.3a, 4.3b and 4.3c respectively. Vegetation is relatively bright in the NIR spectrum image and relatively dim in the visible and UVA spectrum images. However, vegetation in the UVA image appears brighter than vegetation in the visible image due to the narrow NIR radiation band transmittance characteristic of the UVA-pass filter.



Figure 4.3. Scene 1 in the (a) NIR, (B) visible and (c) UVA spectrums.

False color techniques are commonly used to monitor environmentally significant resources such as agriculture and forest acreage. The monochromatic images of Figure 4.3 were assigned false color and combined to form a single RGB false color image that represented the UVA, visible and NIR spectrums; essentially, extending the “visible” spectrum into the UVA and NIR spectrums. The NIR spectrum image from Figure 4.3a was false colored monochromatic red, the visible spectrum image from Figure 4.3b was false colored monochromatic green and the UVA spectrum image from Figure 4.3c was false colored monochromatic blue. Figures 4.4, 4.5 and 4.6 contain the original grey-scale images and the associated monochromatic RGB images for the NIR, visible and UVA spectrums respectively.



Figure 4.4. NIR spectrum image (left) grey-scale and (right) monochromatic red.



Figure 4.5. Visible spectrum image (left) grey-scale and (right) monochromatic green.



Figure 4.6 UVA spectrum image (left) grey-scale and (right) monochromatic blue.

Figure 4.7 is a false color RGB image which was created by adding the images presented in Figures 4.4(right), 4.5(right) and 4.6(right). Adding the monochromatic pixel values was appropriate because the RGB color model is an additive model.

Through the false color method the vegetation in the scene can be differentiated from the non-vegetation. Because vegetation appears bright in the UVA and NIR spectrum images and dim in the visible spectrum image, vegetation within the scene changes “color” to become a vibrant purple, pink and red when the three monochromatic images are added. Unlike vegetation, non-vegetation does not appear to change “color” for this unique multispectral false color assignment.



Figure 4.7 False color image created by combining monochromatic RGB images

The false color image in Figure 4.7 allows for the quick, visual identification of vegetation within a scene. Furthermore, the false color technique is insensitive to variable daytime lighting conditions. False color images for Scene 1 and Scene 2 are presented together in Figure 4.8. The NIR, visible and UVA spectrum grey-scale images used to create these false color images were captured on different days and under

different natural lighting conditions. Scene 1 represents false color results for a cloudy day and Scene 2 represents false color results for a sunny day. Vegetation in the two images is consistently represented as purple, pink and red.



Figure 4.8. False color results for (left) Scene 1 and (right) Scene 2.

The autonomous, remote tracking of vegetation growth and senesce through the use of computer vision requires the application of either an RGB or HSL (hue, saturation and luminance) color model threshold. The threshold separates out pixels with a purple, pink or red hue and identifies those pixels as vegetation. The results for a color model threshold applied to Scene 1 and Scene 2 are presented in Figure 4.9.

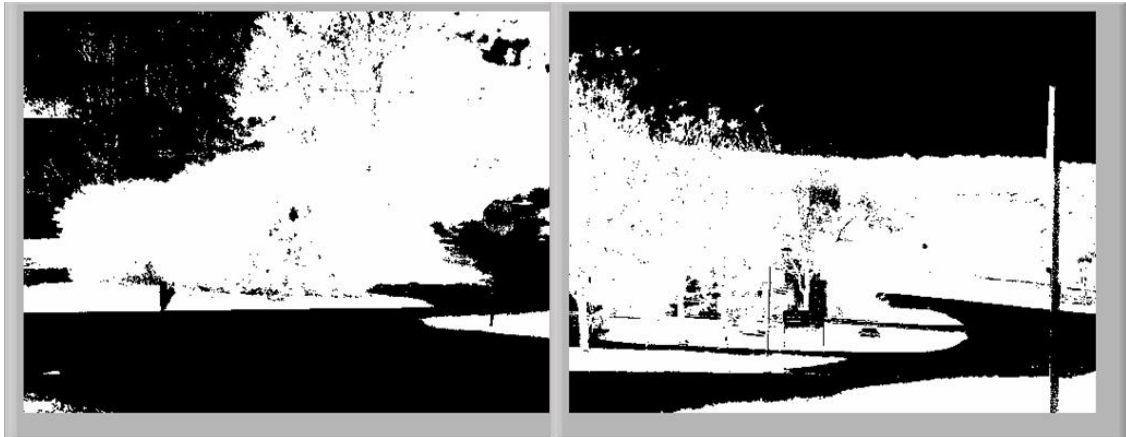


Figure 4.9. Color model threshold results for (left) Scene 1 and (right) Scene 2.

The computing effort required capturing spectrum images, assigning color planes to the images, combining the images and subsequently thresholding the false color image

is substantial if the tracking of vegetation growth and senesce is to be accomplished in real time. A more efficient technique for differentiating between vegetation and non-vegetation is a direct comparison of grey-scale NIR and visible spectrum images. Section 4.2 presents a technique for comparing grey-scale NIR and visible spectrum images for the identification of vegetation within a scene.

4.2 NDVI (Normalized Difference Vegetation Index)

Vegetation can be differentiated from non-vegetation through utilization of the NDVI (Normalized Difference Vegetation Index). Unlike multispectral imaging techniques that extract meaningful data from the combination of entire electromagnetic spectrums, the NDVI uses hyperspectral imaging techniques to measure electromagnetic radiation reflectance at a single red wavelength and a single NIR wavelength. The NDVI is defined as

$$NDVI = \frac{\lambda_{NIR} - \lambda_{Red}}{\lambda_{NIR} + \lambda_{Red}} \quad (1)$$

where λ_{NIR} is 830 nm and λ_{Red} is 680 nm [7]. This equation produces values between -1.0 and 1.0. NDVI values for vegetation, construction materials and ice are presented in Figure 4.10. Reflectance data were taken from the USGS, JHU and JPL spectral libraries. NDVI values for vegetation are centered on 0.8 and construction materials and ice have values between 0 and 0.1. These differences in NDVI values allow vegetation to be differentiated from non-vegetation.

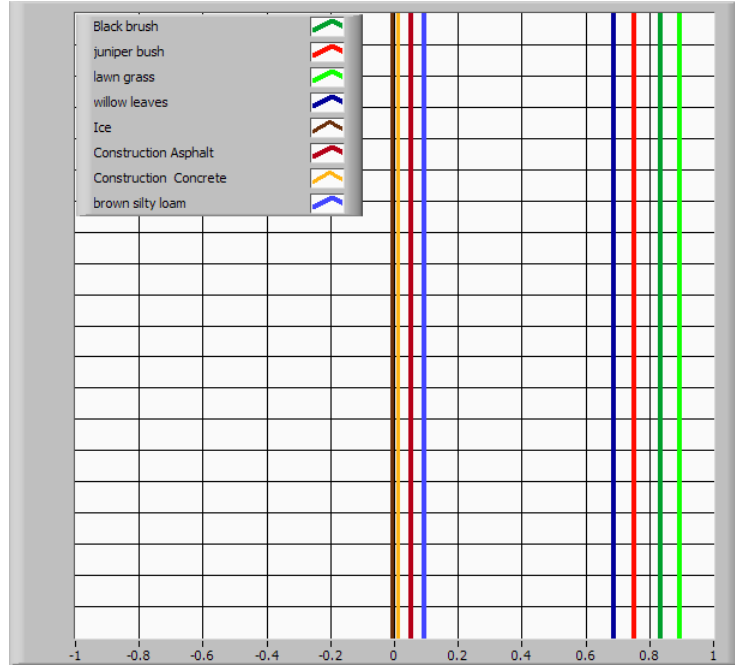


Figure 4.10 NDVI values for vegetation, construction material and ice

Although hyperspectral imaging was used to obtain the data presented in Figure 4.10, a multispectral imaging approach is now proposed for differentiating between vegetation and non-vegetation. The NDVI equation must be adjusted in order to incorporate the visible and NIR spectrum images obtained with the multispectral imaging system described in Section 4.1. The adjusted NDVI uses the entire visible and NIR spectrums and is defined as

$$NDVI^* = \frac{Pix_{NIR} - Pix_{Vis}}{Pix_{NIR} + Pix_{Vis}} \quad (2)$$

where Pix_{NIR} is a pixel value from a NIR spectrum image and Pix_{Vis} is the value of the corresponding pixel in a visible spectrum image. As with the original NDVI, the $NDVI^*$ produces values between -1.0 and 1.0.

$NDVI^*$ values are passed through a threshold filter to separate vegetation values from non-vegetation values within a scene. The hyperspectral NDVI data presented in Figure 4.10 predicted that vegetation values should fall between 0.6 and 0.9. However,

the multispectral $NDVI^*$ data requires this range to be adjusted. Therefore, the $NDVI^*$ images in Figure 4.11 and Figure 4.12 were created by applying a threshold of 0.3 to $NDVI^*$ values for Scene 1 and Scene 2 respectively. Black pixels in Figure 4.11 and Figure 4.12 represent non-vegetation with $NDVI^*$ values below 0.3 and white pixels represent vegetation with $NDVI^*$ values between 0.3 and 0.8.



Figure 4.11 Scene 1 visible spectrum image (left) and $NDVI^*$ solution (right).



Figure 4.12 Scene 2 visible spectrum image (left) and $NDVI^*$ solution (right).

As with the false color technique described in the previous section, the $NDVI^*$ approach to vegetation identification is insensitive to variable daytime lighting

conditions. $NDVI^*$ values between 0.3 and 0.8 consistently represent vegetation in Scene 1 and Scene 2. Scene 1 images were captured on a relatively cloudy day and Scene 2 images were captured on a relatively sunny day. The multispectral $NDVI^*$ approach is also a more time efficient and cost effective method for differentiating between non-vegetation and vegetation within a scene, and is superior to the hyperspectral false color differentiating method described earlier.

The $NDVI^*$ technique can be utilized in real time with an update rate of 10 Hz; whereas, the hyperspectral false color technique presented in Section 4.1 has an update rate of 1 Hz. Hyperspectral imagers, such as Ocean Optics HR4000 spectrometer can be cost prohibitive. The HR4000 spectrometer, collimating lens and reflectance standard for system calibration has a combined system cost of \$5400; excluding annual spectrometer servicing [18]. The proposed multispectral $NDVI^*$ system uses two Sony XCD-X710 cameras, two focusable double Gauss lenses, a visible-pass filter and an infrared-pass filter. The $NDVI^*$ system has a combined cost of \$3500; representing a savings of \$1900 over the hyperspectral NDVI solution [1] [5].

Chapter 5 Vegetation Fluorescence Results

5.1 Equipment

The objective of this experiment is to subjectively determine vegetative health through the utilization of the $NDVI^*$ imaging system developed in Chapter 4. An attempt is made to measure vegetation fluorescence levels through the incorporation of a red light excitation source into the $NDVI^*$ imaging system. Comparison of vegetation fluorescence measurements provides a unique method for subjectively determining photochemical quenching through PSII quantum yield calculations, $\Phi_{PSII} = (F'_m - F_t) / F'_m$, and non-photochemical quenching, $NPQ = (F_m - F'_m) / F'_m$, and, therefore, an insight into photosynthetic efficiencies. PSII quantum yield calculations require the ability to measure maximum vegetation fluorescence and steady-state vegetation fluorescence under actinic excitation. Non-photochemical quenching calculations require the ability to measure maximum dark adapted vegetation fluorescence and maximum vegetation fluorescence under red light excitation in actinic light. Decreases and increases in photosynthetic efficiencies detected through the comparison of fluorescence measurements cannot diagnose specific vegetation stresses; they instead provide a holistic picture of vegetation stress levels.

The adjusted $NDVI^*$ imaging system for measuring vegetation fluorescence is presented in Figure 5.1. The Sony XCD-X710 monochromatic camera is securely mounted on a tripod 240mm above an ebony imaging surface. The mounting height of the camera represents the minimum working distance of the focusable double gauss imaging lens. At a distance of 240mm, the camera field of view is $20mm \times 25mm$. The camera is aligned vertically and has a normal orientation with regard to the imaging surface. The red light excitation source is mounted to a spherical desktop vice at an 45° angle. The Sony XCD-X710 camera and laser diode are controlled through National Instruments LabView software. LabView programs are used to capture images, control diode pulses and store image pixel values.

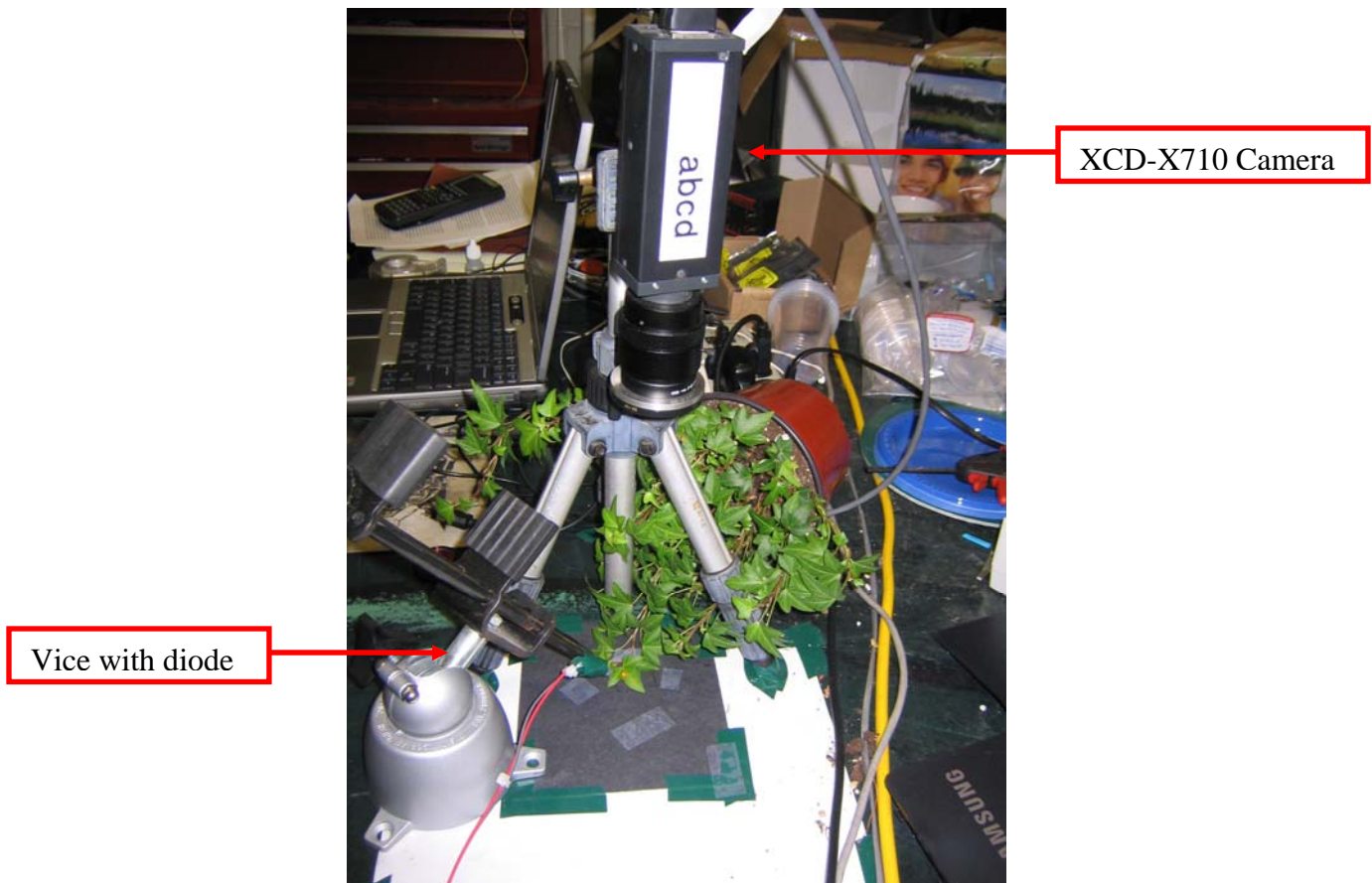


Figure 5.1 Vegetation fluorescence measurement system

The red excitation source is a modified laser pointer manufactured by Quarton Inc [19]. The diode is listed as a class IIIa laser with a maximum output power of 4 mW. The laser pointer provides non-modulated light between 630 nm and 680 nm. To obtain a pulsed excitation source, the diode and electronics board are removed from the original “pointer” packaging (Figure 5.2). The power button is bypassed and the power leads are connected to an external power supply. The diode is pulsed using a digitally controlled BJT (Bipolar Junction Transistor). The schematic for the control circuit is presented in Figure 5.3. The maximum red absorption for chlorophyll *a* is 662 nm; therefore, with regard to electromagnetic frequency, the laser diode is an appropriate source of excitation radiation [16]. The diode footprint is $1\text{mm} \times 4\text{mm}$; representing 0.77% of the imaging surface.



Figure 5.2 Original laser pointer package and laser diode electronics board

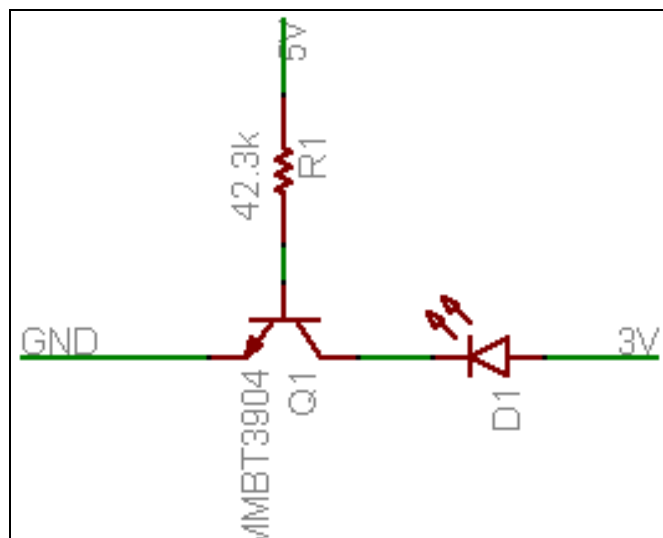


Figure 5.3 Laser diode control circuit

The Sony XCD-X710 camera contains a one-third inch progressive scan IT CCD sensor with a 600×800 pixel resolution, and provides a pixel depth of 10 bits. The imaging sensor is sensitive to wavelengths between 300 nm and 1000 nm; with a maximum relative sensitivity occurring at 500 nm. Chlorophyll *a* fluoresces between 650 nm and 750 nm; with maximum fluorescence occurring at a wavelength of 666 nm. The relative sensitivity of the imaging sensor is 65% and 40% at 650 nm and 750 nm respectively. The IR-pass filter for the $NDVI^*$ imaging system developed in Chapter 4 is designed to pass radiation with wavelengths greater than 700 nm. Relative sensitivity for the imaging sensor at 700 nm is 50%. Therefore, the $NDVI^*$ imaging system IR-pass filter may not be capable of passing a sufficient quantity of vegetation fluorescence radiation for detection by the Sony XCD-X710 imaging sensor.

The Sony XCD-X710 imaging sensor produces a nominal current output even in the absence of radiation; known as dark current. Dark current is a product of the thermal generation of electron-hole pairs at crystalline defects and represents a source of low level system noise [3]. The four commonly accepted sources of dark current are diffusion current, depletion layer generation current, surface generation current and leakage. Dark current values for the Sony XCD-X710 camera are measured with a lens cap rejecting incoming electromagnetic radiation. The mean dark current pixel value for the Sony XCD-X710 camera falls between a pixel value of 40 and 41.

The IR-pass filter for the $NDVI^*$ imaging system is an interference filter designed to reject collimated, non-IR radiation that is oriented normally with respect to the filter plane. As the angle of incident radiation increases, the transmittance profile of the interference filter will shift towards shorter wavelengths [3] [5]. Therefore, a percentage of non-IR radiation with a non-normal orientation will pass through the interference filter resulting in the detection and measurement of far-red spectrum electromagnetic radiation (Figure 5.4). Furthermore, the relative sensitivity of the imaging sensor is greater at far red wavelengths and lesser at NIR wavelengths; resulting in a higher probability for the detection of far red radiation. Visible spectrum radiation passing through the filter contributes to system noise; resulting in a false positive for vegetation fluorescence.

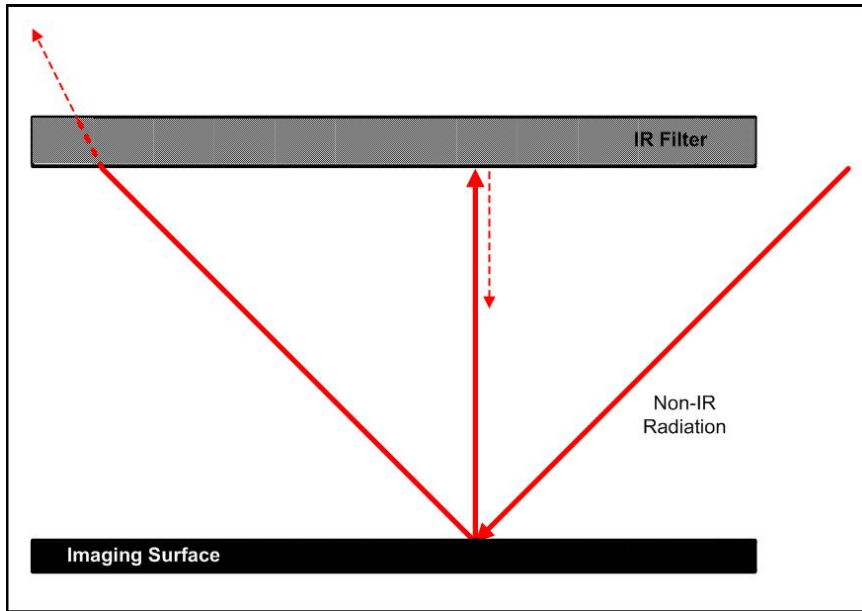


Figure 5.4. Non-IR radiation with a non-normal orientation passing through an interference filter

5.1 Vegetation Fluorescence Measurements

The quantum yield of PSII is directly related to photo-chemical quenching. PSII quantum yield calculations require the measurement of steady-state vegetation fluorescence under actinic excitation. Collection of meaningful steady-state vegetation fluorescence measurements relies on the ability of the Sony XCD-X710 imaging sensor, in combination with the IR-pass filter, to produce representative IR spectrum pixel values for vegetation that are significantly greater than those representing non-vegetation. To this end, IR spectrum pixels for vegetation are compared with dark current pixel values and IR spectrum pixel values for white paper and an ebony imaging surface. A visible spectrum image containing a green leaf, white paper and an ebony imaging surface is presented in Figure 5.5; with the vegetation, white paper and ebony imaging surface labeled and highlighted within the image.

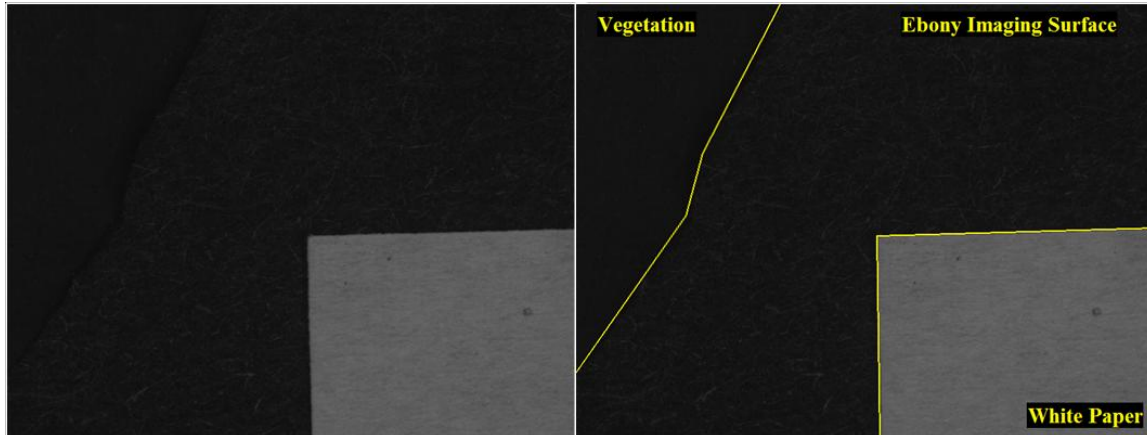


Figure 5.5. Visible spectrum image containing vegetation, white paper and an ebony imaging surface.

Figure 5.6 and Figure 5.7 present the mean IR spectrum pixel values for vegetation, white paper and the ebony imaging surface presented in Figure 5.5. When the vegetation, white paper and ebony imaging surface are sensed through the IR-pass filter, the mean pixel values for each material fall between 40 and 41. Figure 5.7 also presents 300 sequential pixel values and median pixel values for dark current, vegetation, white paper and the ebony imaging surface. The mean and median pixel values were calculated with a sample size equal to 10,000 pixels. The median pixel value for dark current, vegetation, white paper and the ebony imaging surface were equal and had a value of 41. Therefore, IR spectrum pixel values for vegetation are not significantly different than IR spectrum pixel values for dark current, white paper or the ebony imaging surface.

The IR spectrum image used to calculate mean and median pixel values for vegetation, white paper and the ebony imaging surface is presented in Figure 5.8. The image was passed through a threshold with a pixel value equal to 41. Black pixels represent a value less than 41 and white pixels represent a pixel value greater than or equal to 41. Figure 5.8 highlights the inability of the *NDVI** imaging system developed in Chapter 4 to measure steady-state vegetation fluorescence in actinic light under laboratory conditions. The imaging system cannot be used to calculate the quantum yield of PSII and, therefore, is not an appropriate system for determining non-photochemical quenching.

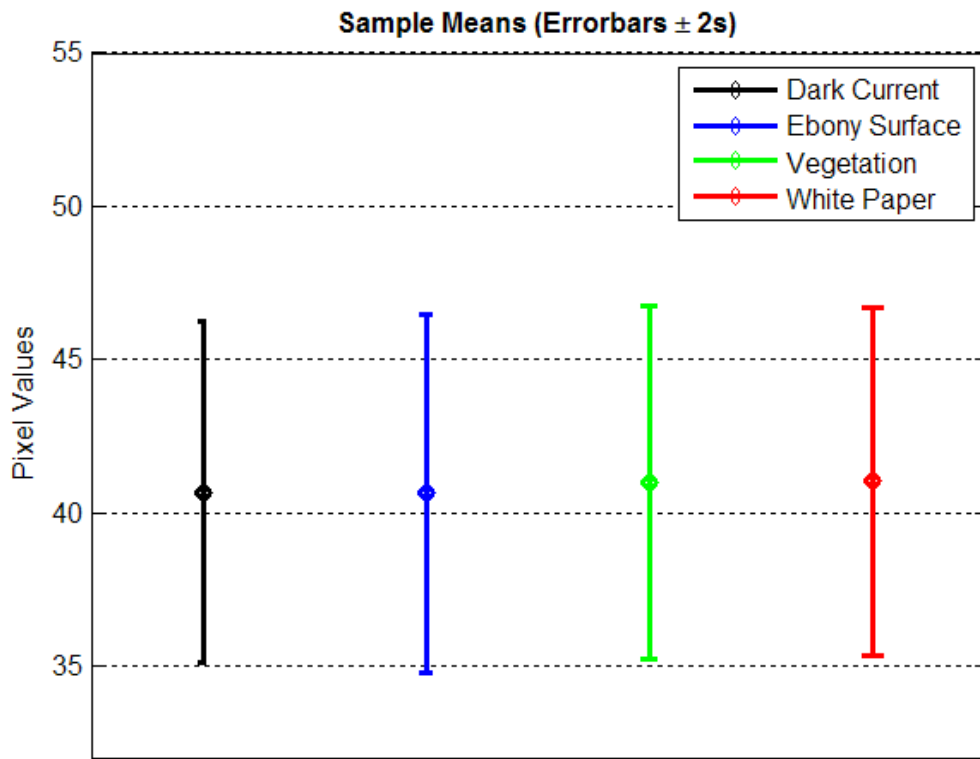


Figure 5.6. Mean IR spectrum pixel values for dark current, vegetation, white paper and an ebony imaging surface.

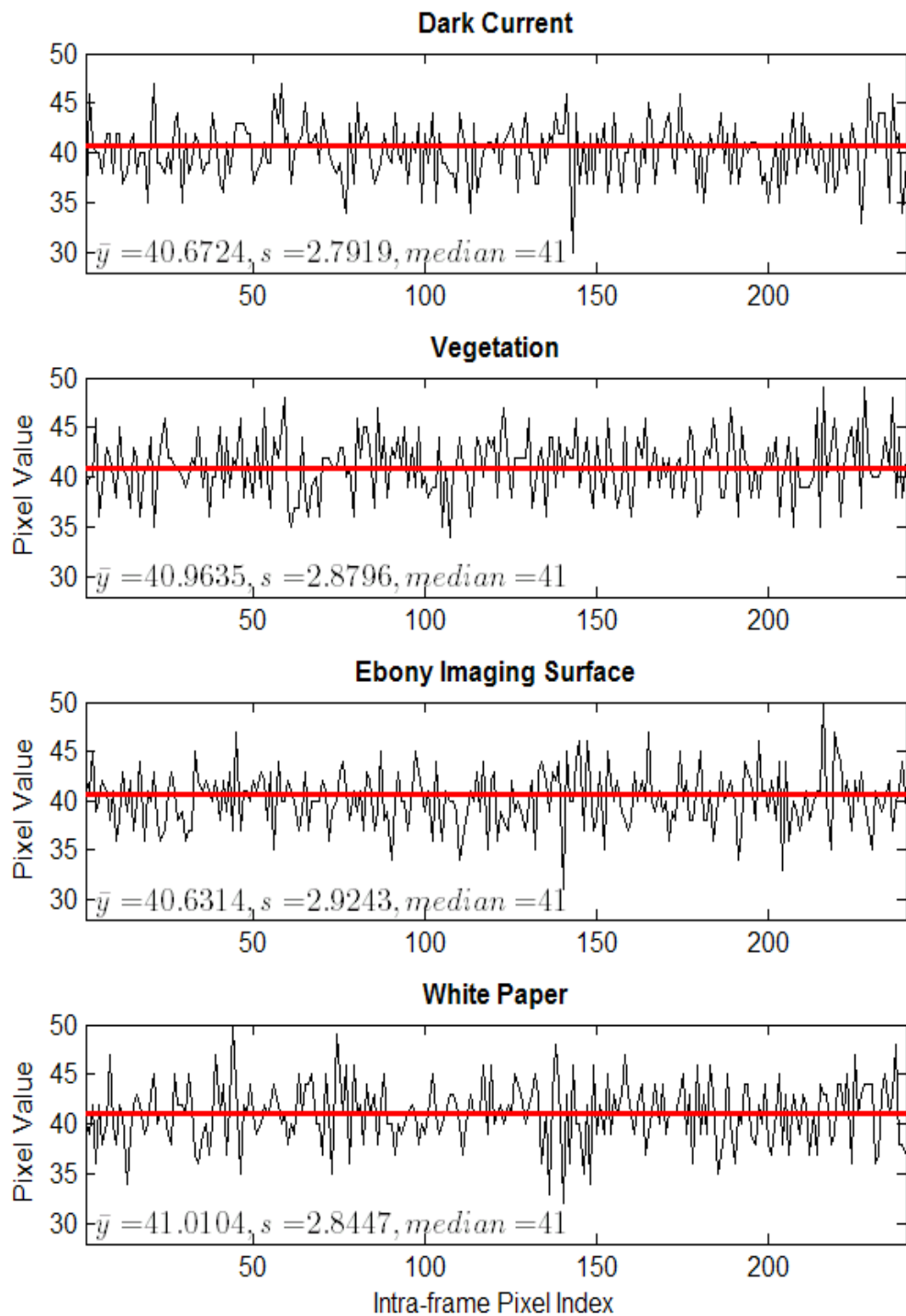


Figure 5.7. Sequential IR spectrum pixel values for dark current, vegetation, white paper and an ebony imaging surface.

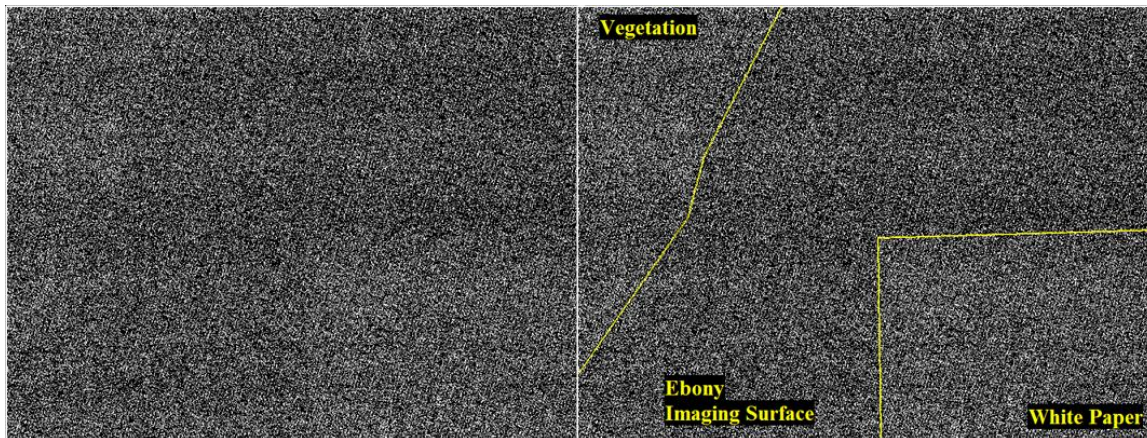


Figure 5.8. Threshold IR spectrum image containing vegetation, white paper and an ebony imaging surface.

Non-photochemical quenching calculations require the ability to measure maximum dark adapted vegetation fluorescence and maximum vegetation fluorescence in actinic light. These maximum fluorescence measurements are recorded with the vegetation under red laser diode excitation. Collection of meaningful maximum vegetation fluorescence measurements under red light excitation in actinic light relies on the ability of the Sony XCD-X710 imaging sensor, in combination with the IR-pass filter, to produce representative IR spectrum pixel values for vegetation under red light excitation in actinic light that are significantly greater than those representing vegetation without red light excitation in actinic light. Figure 5.9 contains a visible spectrum image of a green leaf under red light excitation in actinic light.

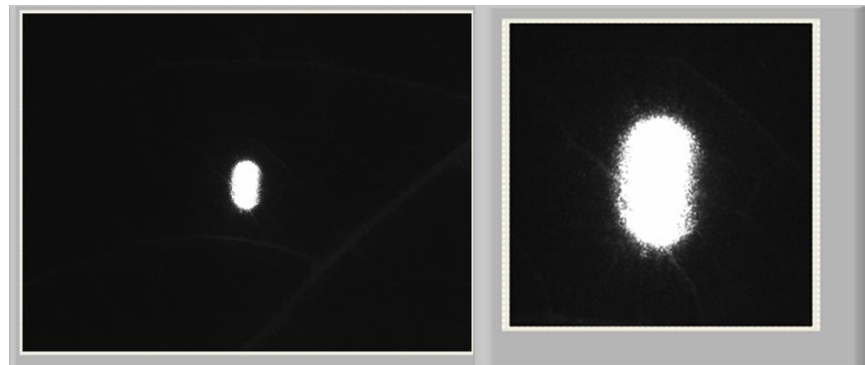


Figure 5.9. Vegetation under red light excitation in actinic light.

Measuring maximum vegetation fluorescence in actinic light requires a red light excitation source to be pulsed periodically. The frequency with which the red light excitation source should be pulsed to insure that the vegetation has relaxed completely to a pre-pulsed state is between 45 min and 60 min [15]. Figure 5.10 presents mean pixel values for vegetation during a single red light excitation pulse and mean pixel values for vegetation under actinic excitation. Each mean was calculated from a sample with size equal to 10,000 pixels. The maximum mean pixel value recorded during red light excitation is equal to 57. The mean pixel value for vegetation under actinic excitation is equal to 41. An increase in pixel value from 41 to 57 represents a 39% increase in relative mean pixel value. When the 10 bit pixel scale is considered the absolute increase in mean pixel value from 41 to 57 represents 1.56% of the full scale. The difference in mean pixel value observed for vegetation under red light excitation in actinic light and vegetation under actinic excitation is minimal. Furthermore, pixel value distributions for vegetation under red light excitation in actinic light and vegetation under actinic light excitation overlap one another. Figure 5.10 highlights this overlap by displaying mean pixel values along with error bars of $\pm 3s$; representing 99.73% of sample pixel values.

The increase in measurable radiation leaving the vegetation surface is a result of interactions between the red light excitation source and all molecules contained within the vegetation. The *NDVI** imaging system records these interactions in toto and is, therefore, unable to distinguish between fluorescence associated with chlorophyll *a* fluorescence and thermal decomposition and photo bleaching.

The *NDVI** imaging system developed in Chapter 4 is not an appropriate system for measuring vegetation fluorescence under red light excitation in actinic light. Therefore, the imaging system cannot be used to calculate non-photochemical quenching under laboratory conditions.

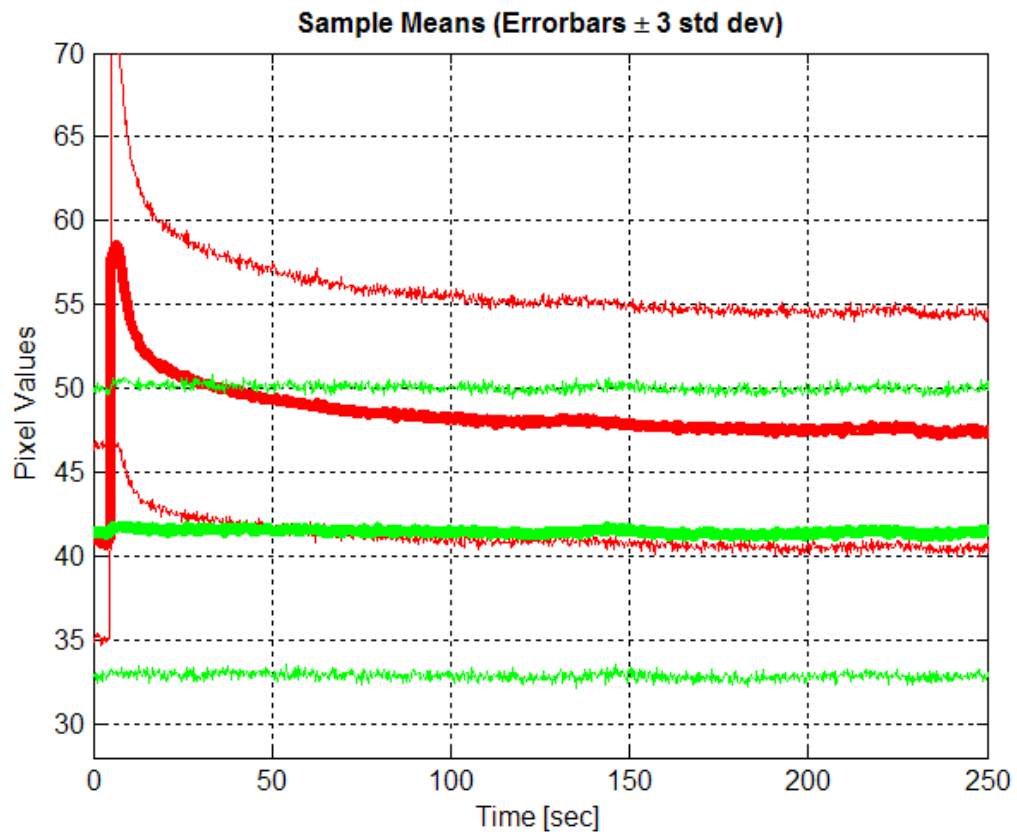


Figure 5.10. Mean pixel values for vegetation during a red light excitation pulse (red) and under actinic excitation (green).

Chapter 6 Conclusions

6.1 NDVI (Normalized Difference Vegetation Index)

The NDVI was developed to differentiate between vegetation and non-vegetation. This index requires hyperspectral imaging equipment and compares radiation with wavelengths equal to 680 nm and 830 nm. The multispectral $NDVI^*$ has been defined and is a variation of the NDVI which utilizes the visible and NIR spectrums in toto. $NDVI^*$ analysis software was developed to quickly differentiate between vegetation and non-vegetation. This method compares a visual spectrum image and an NIR spectrum image of a scene; producing values between -1 and 1 for each image pixel. $NDVI^*$ values falling between 0.3 and 0.8 consistently indicate that an image pixel represents vegetation. $NDVI^*$ values below 0.3 consistently indicate that an image pixel represents non-vegetation. Utilization of the $NDVI^*$ could allow for the real time, remote monitoring of vegetative growth and decay at a frequency of 10 Hz. Furthermore, the $NDVI^*$ technique requires an imaging system with a combined system cost of \$3500. This represents an approximate cost savings of \$1900 over the hyperspectral imaging equipment required for utilization of NDVI methods.

Development of a greenhouse deployable sensor package is the next step in the verification of the $NDVI^*$ imaging system as a robust method for autonomously tracking vegetation growth and status. $NDVI^*$ values for vegetation and non-vegetation need to be compared with direct LAI measurements to assess the accuracy of the proposed multispectral imaging methods.

6.2 Vegetation Fluorescence

Vegetation fluorescence must be carefully measured; failure to do so will result in meaningless and insignificant data [15] [4]. Fluorescence signals vary greatly between plants; as well as between the leaves of a plant. It is therefore imperative that data collected from individual leaves not be interchanged. Subsequent fluorescence measurements are relative to an initial maximum fluorescence potential measured during a dark-adapted state. Because vegetation fluorescence is a relative measurement, it cannot be used as a diagnostic tool; specific stress and damage cannot be ascertained. However, when implemented appropriately, fluorescence is a non-destructive, *in vivo* qualitative method for determining to what extent an environmental stress is affecting photochemistry and heat dissipation.

The *NDVI** imaging system was combined with a red laser diode excitation source in an attempt to measure vegetation fluorescence. Vegetation fluorescence levels can be used to calculate photochemical quenching through PSII quantum yield calculations, $\Phi_{PSII} = (F'_{m} - F_t) / F'_{m}$, and non-photochemical quenching, $NPQ = (F_m - F'_{m}) / F'_{m}$. The system included an IR sensitive CCD, IR-pass filter and a laser diode with mean radiation output equal to 650 nm. LabView software was used to capture and record images at 7.5 fps.

System noise due to dark current and IR-pass filter and imaging sensor sensitivity limitations mean that the *NDVI** imaging system developed in Chapter 4 is an inappropriate solution for the measurement of vegetation fluorescence under actinic excitation and vegetation fluorescence under red light excitation in actinic light. The median value for pixels representing vegetation was equal to median pixel values for dark current, white paper and an ebony imaging surface under actinic excitation. Under red light excitation, the maximum mean pixel value for vegetation increased a mere 1.56% over the mean pixel value for vegetation under actinic excitation. The minimal increase in mean pixel value associated with red light excitation was most likely attributable to thermal decomposition and photo bleaching, and not chlorophyll *a* fluorescence.

References

- [1] Adorama. www.adorama.com
- [2] Barnes, E. M., & M. G. Baker. (2000). Multispectral Data for Mapping Soil Texture: Possibilities and Limitations. *Applied Engineering in Agriculture ASAE 16*, pp 731-741.
- [3] Bass, Michael, ed. A Handbook of Optics: Fundamentals, Techniques, & Design. 2nd ed. New York, NY: McGraw-Hill, 1995. pp 22.12-22.13.
- [4] DeEll, Jennifer and Peter M. A. Toivonen, ed. Practical Applications of Chlorophyll fluorescence in Plant Biology. Norwell, Mass USA: Academic Publishers, 2003.
- [5] Edmund Optics. www.edmundoptics.com/US
- [6] Fenner, Michael, ed, Seeds: The Ecology of Regeneration in Plant Communities. New York, NY: CABI Publishing, 2000. pp 31.
- [7] Fogler, Joseph R. (2003) Multi- and Hyper-Spectral Sensing for Autonomous Ground Vehicle Navigation. *Sandia National Labs*, Sandia Report SAND, 2003. pp 25-29.
- [8] Food and Agriculture Organization of the United Nations. Agriculture and Horticultural Seeds. Rome, 1961. pp 107-109.
- [9] Islam, Kamrunnahar, Alex McBratney, & Balwant Singh. (2005). Rapid estimation of soil variability from the convex hull biplot area of topsoil ultra-violet, visible and near-infrared diffuse reflectance spectra. *GEODERMA*, 128, pp 249-257.
- [10] Jalink, Henk, Rob van der Schoor, Angela Frandas, & Jaap G. van Pijlen. (1998). Chlorophyll fluorescence of *Brassica oleracea* seeds as a non-destructive marker for seed maturity and seed performance. *Seed Science Research*, 8, pp 437-443.
- [11] Jalink, H., R. van der Schoor, Y. E. Birnbaum, & R. J. Bino. (1999). Seed Chlorophyll Content As An Indicator For Seed Maturity And Seed Quality. *Acta Horticultur Proceedings of the Sixth Symposium on Stand Establishment and ISHS Seed Symposium*, 504, pp 219-228.
- [12] L. F. Johnson, D. E. Roczen, S. K. Youkhana, R. R. Nemani & D. R. Bosch. (2002) Mapping Vineyard Leaf Area with Multispectral Satellite Imagery. *Computers and Electronics in Agriculture* 38, pp 33-44.
- [13] Lu, R. (2001). Predicting Firmness and Sugar Content of Sweet Cherries Using Near-Infrared Diffuse Reflectance Spectroscopy. *Transactions of the ASAE*, 44(5), pp 1265-1271.
- [14] Lu, Renfu, & Yankun Peng. (2005). Hyperspectral Scattering for assessing Peach Fruit Firmness. *Biosystems Engineering*, 1537-5110.
- [15] Maxwell, Kate, & Giles N. Johnson. (2000). Chlorophyll fluorescence – a practical guide. *Journal of Experimental Botany*, 51 pp 659-668.
- [16] Nobel, Park S. *Physicochemical & Environmental Plant Physiology*. San Diego, California: Academic Press, 1999. pp 158.
- [17] Noble, Scott D., & Ralph B. Brown. (2004). Plant Identification Using Hyperspectral and Multi-Perspective Imaging. *ASAE/CSAE Meeting Presentation*, 041074.
- [18] Ocean Optics. www.oceanoptics.com.
- [19] Quarton Inc. <http://www.quarton.com>.

- [20] Pan, Zhihong, Gleen Healey, Manish Prasad, & Bruce Tromberg. (2003). Face Recognition in Hyperspectral Images. *IEEE Transactions on Pattern Analysis and Machine Intelligence*, 25(12), pp 1552-1560.
- [21] Strachan, Ian B., Elizabeth Pattey, & Johanne B. Boisvert. (2002). Impact of nitrogen and environmental conditions on corn as detected by hyperspectral reflectance. *Remote Sensing of Environment*, 80, pp 213-224.
- [22] Turner Designs. www.turnerdesigns.com.
- [23] United States Geological Survey. <http://edc.usgs.gov/products/satellite/avhrr.html#prices>
- [24] Wilhelmus A. C. M. Messelink, Klamer Schutte, Albert M. Vossepoel, Frank Cremer, John G.M. Schavemaker & Eric den Breejen. Feature-based detection of landmines in infrared images. *Proceedings of SPIE* Vol 4742, 2002. pp1.